

# IMAGE AUGMENTATION WITH CONFORMAL MAPPINGS FOR A CONVOLUTIONAL NEURAL NETWORK

OONA RAINIO, MOHAMED M.S. NASSER, MATTI VUORINEN, AND RIKU KLÉN

**ABSTRACT.** For augmentation of the square-shaped image data of a convolutional neural network (CNN), we introduce a new method, in which the original images are mapped onto a disk with a conformal mapping, rotated around the center of this disk and mapped under such a Möbius transformation that preserves the disk, and then mapped back onto their original square shape. This process does not result the loss of information caused by removing areas from near the edges of the original images unlike the typical transformations used in the data augmentation for a CNN. We offer here the formulas of all the mappings needed together with detailed instructions how to write a code for transforming the images. The new method is also tested with simulated data and, according the results, using this method to augment the training data of 10 images into 40 images decreases the amount of the error in the predictions by a CNN for a test set of 160 images in a statistically significant way (p-value=0.0360).

## Author information.

Oona Rainio<sup>1</sup>, email: [ormrai@utu.fi](mailto:ormrai@utu.fi), ORCID: 0000-0002-7775-7656

Mohamed M.S. Nasser<sup>2</sup>, email: [mms.nasser@wichita.edu](mailto:mms.nasser@wichita.edu)

Matti Vuorinen<sup>3</sup>, email: [vuorinen@utu.fi](mailto:vuorinen@utu.fi), ORCID: 0000-0002-1734-8228

Riku Klén<sup>1</sup>, email: [riku.klen@utu.fi](mailto:riku.klen@utu.fi), ORCID: 0000-0002-0982-8360

1: Turku PET Centre, University of Turku and Turku University Hospital, Turku, Finland

2: Department of Mathematics, Statistics, and Physics, Wichita State University, Wichita, KS 67260-0033, USA, and Department of Mathematics, Statistics, and Physics, Qatar University, Doha, Qatar

3: Department of Mathematics and Statistics, University of Turku, Turku, Finland

**Code availability.** Available at [https://github.com/rklen/Conf\\_map\\_augmentation](https://github.com/rklen/Conf_map_augmentation)

**Data availability.** Data will be made available at reasonable request.

**Conflict of interest.** On the behalf of all authors, the corresponding author states that there is no conflict of interest.

**Funding.** The first author was financially supported by the Finnish Culture Foundation.

**Acknowledgments.**

---

File: main.tex, printed: 2022-12-13, 2.03

*Key words and phrases.* Conformal mapping, convolutional neural network, deep learning, image augmentation.

## 1. INTRODUCTION

A convolutional neural network (CNN) is a type of deep learning technique that is well-suited for processing images. It receives image data in a matrix format so that each element of the matrix corresponds to the value of one pixel in the image and then transforms this input through several layers by taking into account the spatial relationships between the data points. The CNNs have been noted to be very useful in different areas of research but training even a single CNN often requires a large number of labelled images, which can sometimes be difficult to obtain.

One possible solution to this problem is using data augmentation, which means that the existing data is multiplied by using simple transformations to create new, slightly different versions of images. Typical transformations used for this purpose are rotations, reflections, and translations but they do not suit for all types of data. Namely, if the image is square-shaped, creating a new version of it with a translation always crops out some areas from the image close to its edges and there are only seven new images that can be created with such a rotation or a reflection that fully preserves the original square. Clearly, the issue would not be encountered if the images given to the CNN would be disk-shaped but this is rarely the case.

However, according to the Riemann mapping theorem from classical function theory, any simply connected proper subdomain of the complex plane can be mapped onto the unit disk with a conformal mapping and, in particular, a conformal mapping called a Schwarz-Christoffel mapping can be used to map a two-dimensional disk onto the interior of a simple polygon [7]. Conformal mappings are much studied in complex analysis because they have many desirable properties such as preserving the magnitudes and directions of angles between curves even though they can turn straight line segments into circular arcs and vice versa. Furthermore, another subtype of conformal mappings are Möbius transformations which can be defined so that they map the interior of a disk onto itself but still significantly transform its contents. While conformal mappings could potentially be utilized in image data augmentation, their formulas are generally quite complicated and require integration of complex valued functions that cannot be computed directly with the existing functions in common programming languages.

In this article, we study if image augmentation can be performed by first mapping each square-shaped image onto a disk with a conformal mapping, then applying such rotations and Möbius transformations that preserve this disk, and finally mapping the resulting images back onto their original shape. First, in Section 2, we present the usual formulas of conformal mappings and other mathematical theory needed. In Section 3, we show how these mappings can be written in Python or other programming languages and how images can be mapped with them. In Section 4, we test this method with one simple example about a CNN predicting a simulated data set. All the codes written in Python and MATLAB are also publicly available so the readers can access to these codes.

## 2. PRELIMINARIES

Let  $G$  be the interior of the square with the vertices  $1 + i, -1 + i, -1 - i, 1 - i$ . In other words, define  $G = \{z \in \mathbb{C} \mid -1 < \operatorname{Re}(z) < 1, -1 < \operatorname{Im}(z) < 1\}$ , where  $\mathbb{C}$  is the complex plane. Denote the unit disk  $\{z \in \mathbb{C} \mid |z| < 1\}$  by  $\mathbb{B}^2$ .

Consider the complete elliptic integrals of the first kind  $\mathcal{K}(r)$  and  $\mathcal{K}'(r)$  defined for  $r \in (0, 1)$  by [3]

$$(2.1) \quad \mathcal{K}(r) = \int_0^1 \frac{dt}{\sqrt{(1-t^2)(1-r^2t^2)}}, \quad \mathcal{K}'(r) = \mathcal{K}(r'), \quad r' = \sqrt{1-r^2}.$$

In many references, the complete elliptic integrals of the first kind  $\mathcal{K}(r)$  is defined as in (2.1), see e.g., See [4, 6, 11]. However, in this paper, we will use the notations used in [1]. Thus, the complete elliptic integrals of the first kind is defined by [1, p. 590]

$$(2.2) \quad \mathcal{K}(m) = \int_0^1 \frac{dt}{\sqrt{(1-t^2)(1-mt^2)}}, \quad \mathcal{K}'(m) = \mathcal{K}(m_1),$$

where  $m = r^2 \in (0, 1)$  and  $m_1 = 1 - m$ . The incomplete elliptic integral of the first kind is defined by [1]

$$(2.3) \quad F(\varphi, m) = \int_0^\varphi \frac{d\theta}{\sqrt{1-m\sin^2\theta}} = \int_0^{\sin\varphi} \frac{dt}{\sqrt{(1-t^2)(1-mt^2)}},$$

and then  $\mathcal{K}(r) = F(\pi/2, m)$ . See [1, 3, 4, 6, 11] for more information.

The Jacobian elliptic functions can be defined with the help of the incomplete elliptic integral (2.3), see [1, Ch. 16]. If

$$\phi = \int_0^\varphi \frac{d\theta}{\sqrt{1-m\sin^2\theta}},$$

then the angle  $\varphi$  is called the *Jacobi amplitude* and we write

$$\varphi = \operatorname{am}(\phi|m).$$

Then the Jacobian elliptic functions are defined by

$$(2.4) \quad \operatorname{sn}(\phi|m) = \sin \varphi, \quad \operatorname{cn}(\phi|m) = \cos \varphi, \quad \operatorname{dn}(\phi|m) = \sqrt{1-m\sin^2(\phi|m)}.$$

The exact conformal mapping from the square region  $G$  and its inverse can be written in terms of the elliptic functions and the incomplete elliptic integral. It follows from [10, p. 182] and [11, p. 242] that the conformal mapping  $f$  from the domain  $G$  onto the unit disk  $\mathbb{B}^2$ ,  $f : G \rightarrow \mathbb{B}^2$ , is given by

$$(2.5) \quad f(z) = \frac{1}{\sqrt{2}e^{i\pi/4}} \frac{\operatorname{sn}(\sqrt{2}Lz|m)}{\operatorname{dn}(\sqrt{2}Lz|m)}, \quad z \in G,$$

where

$$(2.6) \quad r = \frac{1}{\sqrt{2}}, \quad m = r^2, \quad L = \frac{1}{2}\mathcal{K}(m)e^{\pi i/4}.$$

Note that  $\mathcal{K}(m) = \mathcal{K}(1/2) = \Gamma(1/4)^2/(4\pi)$ , see [3, (3.19), p. 51]. Then, it follows from (2.4) and (2.5) that the inverse of this mapping,  $f^{-1} : \mathbb{B}^2 \rightarrow G$ , is given

$$(2.7) \quad f^{-1}(z) = \frac{1}{\sqrt{2}L} F\left(\frac{\sqrt{2}e^{\pi i/4}z}{\sqrt{1+z^2\mathbf{i}}}, m\right), \quad z \in \mathbb{B}^2,$$

which is a conformal mapping from the unit disk  $\mathbb{B}^2$  onto the square domain  $G$ .

Denote the extended complex space by  $\overline{\mathbb{C}} = \mathbb{C} \cup \{\infty\}$  and choose some  $\alpha \in \mathbb{B}^2$ . Define the Möbius transformation  $g : \overline{\mathbb{C}} \rightarrow \overline{\mathbb{C}}$ ,

$$(2.8) \quad g(z) = \frac{z - \alpha}{1 - \bar{\alpha}z}, \quad z \in \mathbb{C},$$

where  $\bar{\alpha}$  is the complex conjugate of  $\alpha$ . This mapping  $g$  fulfills  $g(\mathbb{B}^2) = \mathbb{B}^2$ ,  $g(\alpha) = 0$ , and  $g(0) = -\alpha$ , which means that it preserves the unit disk  $\mathbb{B}^2$  but is not an identity mapping as long as  $\alpha \neq 0$ .

Finally, we define formally the rotation about the origin for an angle  $k \in [0, 2\pi)$  as  $v : \mathbb{C} \rightarrow \mathbb{C}$ ,

$$(2.9) \quad v(z) = ze^{ki}, \quad z \in \mathbb{C}.$$

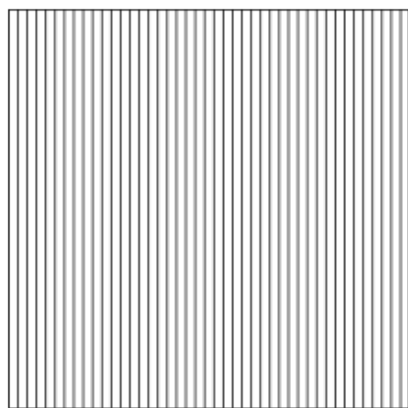
Figure 1 represents visually how the functions  $f$ ,  $g$ , and  $v$  and the inverse function  $f^{-1}$  affect the shape of an image, when  $g$  and  $v$  are defined with constants  $\alpha = 0.3 + 0.3\mathbf{i}$  and  $k = \pi/3$ , respectively.

### 3. CODE

Computing the mapping function  $f$  by (2.5) and its inverse function  $f^{-1}$  by (2.7) requires computing the Jacobian elliptic functions  $\text{sn}(\phi|m)$  and  $\text{dn}(\phi|m)$  for complex  $\phi$  as well as computing the incomplete elliptic integral  $F(\varphi, m)$  for complex  $\varphi$ . Thus, the function  $f$  and its inverse function  $f^{-1}$  cannot usually be computed directly from their definitions (2.5) and (2.7) in the code because the functions used to evaluate the elliptic integrals are not defined for complex numbers in many programming languages. For instance, the complete elliptic integral  $\mathcal{K}(m)$ , the incomplete elliptic integral  $F(\varphi, m)$ , as well as the Jacobian elliptic functions  $\text{sn}(\phi|m)$ ,  $\text{cn}(\phi|m)$ , and  $\text{dn}(\phi|m)$  can be computed for real arguments, with the functions `ellipk`, `ellipkinc`, and `ellipj` of the subpackage `special` of the package `Scipy` [16] in Python. So, in this paper, we will use the properties of the Jacobian elliptic functions and the incomplete elliptic integral to compute their values without the need to compute elliptic integrals of complex variables. For example, the functions  $\text{sn}(z|m)$  and  $\text{dn}(z|m)$ , for a complex variable  $z = x + iy$  where  $x$  and  $y$  are real variables, can be computed using the following formulas [1, §16.21.1]

$$(3.1) \quad \text{sn}(z|m) = \frac{s_0 d_1 + \mathbf{i} c_0 d_0 s_1 c_1}{\delta}$$

$$(3.2) \quad \text{dn}(z|m) = \frac{d_0 c_1 d_1 - \mathbf{i} m s_0 c_0 s_1}{\delta}$$



(A) Original line image

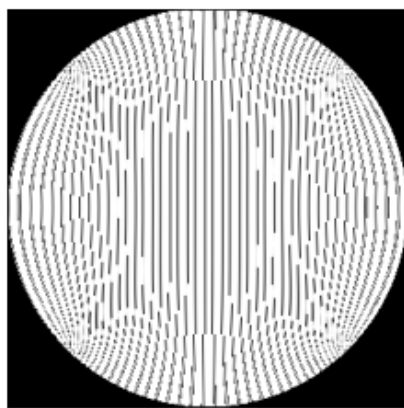
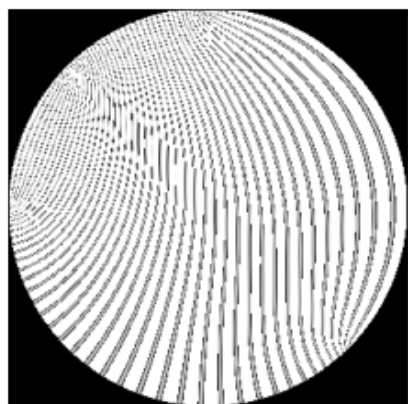
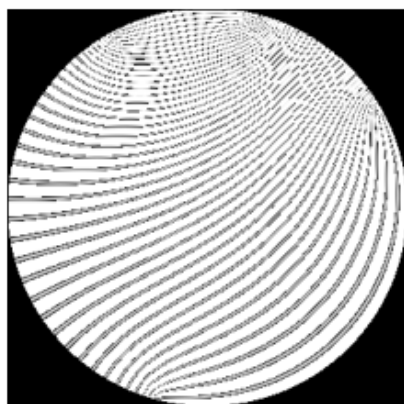
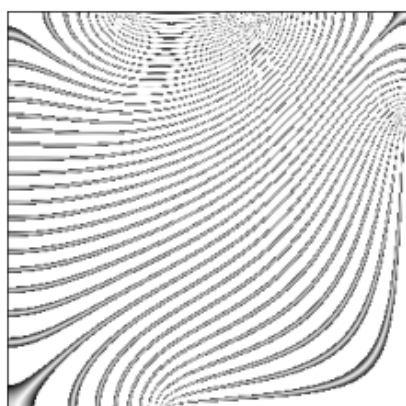
(B) Image after the mapping  $f$ (C) Image after  $g \circ f$ (D) Image after  $v \circ g \circ f$ (E) Image after  $f^{-1} \circ v \circ g \circ f$ 

FIGURE 1. An image of parallel line segments before and after different mappings, including the conformal mapping  $f$  from the original square onto the unit disk, the Möbius transformation  $g$  defined with  $\alpha = 0.3 + 0.3i$ , a rotation  $v$  with  $k = \pi/3$ , and the inverse mapping  $f^{-1}$ .

where

$$\begin{aligned} s_0 &= \operatorname{sn}(x|m), & c_0 &= \operatorname{cn}(x|m), & d_0 &= \operatorname{dn}(x|m), \\ s_1 &= \operatorname{sn}(y|1-m), & c_1 &= \operatorname{cn}(y|1-m), & d_1 &= \operatorname{dn}(y|1-m), \end{aligned}$$

and

$$\delta = c_1^2 + m s_0^2 s_1^2.$$

Similarly, for a complex variable  $z = x + iy$ , the incomplete elliptic integral  $F(z, m)$  can be computed by [1, §17.4.11]

$$(3.3) \quad F(z|m) = F(x + iy|m) = F(x_1|m) + i F(y_1|m_1)$$

where  $x_1$  and  $y_1$  are real variables such that  $X = \cot^2 x_1$  is the positive root of the equation

$$(3.4) \quad X^2 - [\cot^2(x) + m \sinh^2(y) \csc^2(x) - m_1] X - m_1 \cot^2(x) = 0,$$

and  $\tan^2 y_1$  is given by

$$(3.5) \quad \tan^2 y_1 = (\tan^2 x \cot^2(x_1) - 1) / m.$$

Note that, if  $b = -[\cot^2(x) + m \sinh^2(y) \csc^2(x) - m_1]$  and  $c = -m_1 \cot^2(x)$ , then  $c \leq 0$  and hence  $\sqrt{b^2/4 - c} \geq b/2$ . Thus, we have

$$(3.6) \quad \cot^2 x_1 = -b/2 + \sqrt{b^2/4 - c}.$$

Denote below the floor and the ceiling functions with  $\operatorname{floor}()$  and  $\operatorname{ceil}()$ . Then, the values of  $x_1$  and  $y_1$  can be computed from (3.6) and (3.5), respectively, through (see [12])

$$(3.7) \quad x_1 = \operatorname{sign}(\cot(x)) \cot^{-1} \sqrt{-b/2 + \sqrt{b^2/4 - c}} + \pi \operatorname{ceil}(x/\pi - 0.5)$$

$$(3.8) \quad y_1 = \operatorname{sign}(y) \tan^{-1} \sqrt{(\tan^2 x \cot^2(x_1) - 1) / m}.$$

At the beginning of the code, fix the constants  $r$ ,  $m$ , and  $L$  as in (2.6). The conformal mapping  $f$  from the square  $G$  onto the unit disk can now be written with the following pseudo-code.

$$\begin{aligned}
(3.9) \quad & \text{define } f(z) : \\
& \hat{z} = \sqrt{2}Lz \\
& x = \operatorname{Re} \hat{z}; \quad y = \operatorname{Im} \hat{z} \\
& s_0 = \operatorname{sn}(x|m), \quad c_0 = \operatorname{cn}(x|m), \quad d_0 = \operatorname{dn}(x|m), \\
& s_1 = \operatorname{sn}(y|1-m), \quad c_1 = \operatorname{cn}(y|1-m), \quad d_1 = \operatorname{dn}(y|1-m), \\
& \delta = c_1^2 + ms_0^2s_1^2 \\
& \operatorname{sni} = (s_0d_1 + i c_0d_0s_1c_1)/\delta \\
& \operatorname{dni} = (d_0c_1d_1 - i ms_0c_0s_1)/\delta \\
& w = \frac{\operatorname{sni}}{\sqrt{2} e^{\pi i/4} \operatorname{dni}} \\
& \text{return}(w)
\end{aligned}$$

Finding the inverse mapping  $f^{-1}$  requires solving the quadratic equation (3.4). The more unusual trigonometric functions such  $\cot$  or  $\csc$  and their inverses are in the package **sumpy** in Python. Note also that the parameter  $\epsilon$  can be chosen to be any small positive number.

(3.10)

```

define   $f^{-1}(z)$  :
     $\hat{z} = \frac{\sqrt{2}e^{\pi i/4}z}{\sqrt{1+z^2i}}$ 
     $\tilde{z} = \arcsin(\hat{z})$ 
     $x = \operatorname{Re} \tilde{z}; \quad y = \operatorname{Im} \tilde{z}; \quad \epsilon = 0.00001$ 
    #To avoid singularity of  $\cot(x)$  at zero add  $\epsilon$ 
    if  $|x| < \epsilon$  :
         $x = \epsilon$ 
    #Find the roots of the equation (3.4)
     $b = -[\cot^2(x) + m \sinh^2(y) \csc^2(x) - m_1]; \quad c = -m_1 \cot^2(x)$ 
     $X_1 = -b/2 + \sqrt{b^2/4 - c}$ 
     $x_1 = \operatorname{arccot}(\sqrt{X_1})$ 
    if  $X_1 \tan^2(x) < 1$  :
         $y_1 = 0$ 
    else :
         $y_1 = \arctan\left(\sqrt{(X_1 \tan^2(x) - 1)/m}\right)$ 
    #Change of variables taking into account the periodicity ceil to the right
     $x_1 = (-1)\operatorname{floor}(2x/\pi)x_1 + \pi\operatorname{ceil}(x/\pi - 0.5 + \epsilon); \quad y_1 = \operatorname{sign}(y)y_1$ 
     $F_1 = F(x_1, m); \quad F_2 = F(y_1, 1 - m)$ 
     $w = (F_1 + i F_2)/(\sqrt{2}L)$ 
    return( $w$ )

```

After writing the functions  $f$  and  $f^{-1}$  with the pseudo-codes (3.9) and (3.10), they can be tested by choosing a random number  $z$  from the square  $G$ , computing  $w = f(z)$  and  $z' = f^{-1}(w)$ , and printing the difference  $z - z'$ , which should be very close to zero.

An image can be mapped conformally onto a disk with the function `squareToDisk` presented in (3.11). First, suppose then that there is a square matrix called `img` which can be read as a square-shaped grayscale image by choosing the colour of each pixel according the corresponding element in `img`. Let  $h$  be the number of rows or columns in the matrix `img`, `imgH` a vector containing  $h$  evenly spaced points in the interval  $[-1, 1]$ , and  $u$  the distance between two adjacent points in `imgH`. Then we initialize the new image `img` by creating a zero matrix of the same size as `img`. After that, we create a loop that goes through each element of `img` and expresses it as a point  $z \in G$  with the help



of the vector  $\text{imgH}$ . If the point  $z$  belongs to the unit disk, we use the inverse mapping  $f^{-1}$  to find the point  $w$  in the square  $G$  that becomes  $z$  when the domain  $G$  is mapped conformally to the unit disk with the mapping  $f$ . For this point  $w$ , we find such points  $j_0, k_0 \in (0, 1, \dots, h-1)$  and  $j_1, k_1 \in [0, u)$  that  $w = j_0 + j_1 + (k_0 + k_1)i$ , which gives us also the closest four points to  $w$  that correspond to the pixel locations of the original image matrix  $\text{img}$  and the distances between  $w$  and these locations. Finally, we compute the values of the pixel at the point  $w$  by using the weighted means of the four surrounding pixels and, since  $z = f(w)$ , we have the value of the pixel at the point  $z$  in the unit disk.

$$\begin{aligned}
 &\text{define } \text{squareToDisk}(\text{img}) : \\
 &\quad h = \text{dim}(\text{img})[0] \\
 &\quad \text{imgH} = \frac{2}{h-1}(0, 1, \dots, h-1) - (1, \dots, 1) \\
 &\quad u = \text{imgH}[1] - \text{imgH}[0] \\
 &\quad \text{img1} = 0_{\text{dim}(\text{img})} \\
 &\quad \text{for } j \text{ in } (0, 1, \dots, h-1) : \\
 &\quad \quad \text{for } k \text{ in } (0, 1, \dots, h-1) : \\
 &\quad \quad \quad z = \text{imgH}[j] + \text{imgH}[k]i \\
 &\quad \quad \quad \text{if } |z| < 1 : \\
 &\quad \quad \quad \quad w = f^{-1}(z) \\
 &\quad \quad \quad \quad j_0 = \text{floor}((\text{Re}(w) + 1)/u) \\
 &\quad \quad \quad \quad j_1 = (\text{Re}(w) + 1)/u - j_0 \\
 &\quad \quad \quad \quad k_0 = \text{floor}((\text{Im}(w) + 1)/u) \\
 &\quad \quad \quad \quad k_1 = (\text{Im}(w) + 1)/u - k_0 \\
 &\quad \quad \quad \quad \text{img1}[j, k] = j_1 k_1 \text{img}[j_0, k_0] + (1 - j_1) k_1 \text{img}[j_0 + 1, k_0] + \\
 &\quad \quad \quad \quad \quad j_1 (1 - k_1) \text{img}[j_0, k_0 + 1] + \\
 &\quad \quad \quad \quad \quad (1 - j_1)(1 - k_1) \text{img}[j_0 + 1, k_0 + 1]
 \end{aligned}
 \tag{3.11}$$

The function in (3.11) returns such an image matrix that has the original image mapped onto the largest possible disk fitting inside the square-shaped image matrix, and the other values outside this disk are zeroes. Note that this function can be extended for also colour images of RGB or another similar format by just computing the weighted means for the values of each color channel at the end of the loop. Similarly, by replacing the inverse function  $f^{-1}$  with either the Möbius transformation  $g$  of (2.8) or the rotation  $v$  of (2.9), we can map the input image so that the part inside the disk is transformed. To create the function that conformally maps the interior of this disk in the square-shaped image matrix onto the whole matrix, we need to just remove the condition  $|z| < 1$  and replace

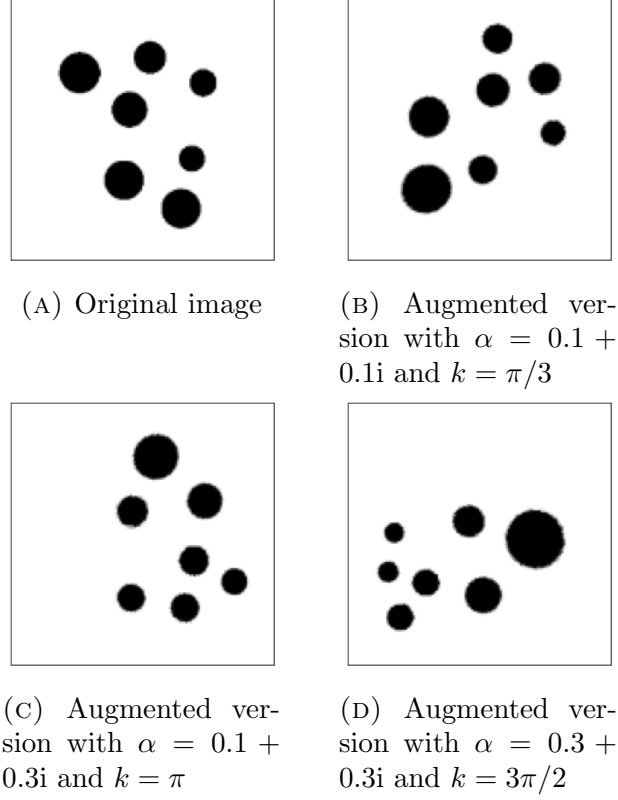


FIGURE 2. An image with  $n = 7$  disks and three augmented versions of this image that have been created with the composed mapping  $f^{-1} \circ v \circ g \circ f$ , where the mappings  $f, g, v$  are as (2.5)-(2.9) for the specified choices of  $\alpha$  and  $k$ .

$w = f^{-1}(z)$  by  $w = f(z)$  in the code (3.11). Alternatively, we can use for instance the composed mapping  $w = (f^{-1} \circ v \circ g \circ f)^{-1}(z) = f^{-1} \circ g \circ v \circ f(z)$  to obtain the image of Figure 1(E).

#### 4. EXPERIMENT

Here, we build a CNN for predicting how many small black disks an otherwise white image contains by using Python (version: 3.9.9) [15] with packages TensorFlow (version: 2.7.0) [2], Keras (version: 2.7.0) [5], and SciPy [16] (version: 1.7.3).

**4.1. Data.** The data set consisted of a set images of from one to ten black disks on white background and an explaining variable containing the correct number of disks for each image. For a number  $n = 1, \dots, 10$ , a single image was created by first initializing a  $300 \times 300$  null matrix corresponding to the domain  $G$ , choosing  $n$  centers  $c_j \in [-0.7, 0.7] \times [-0.7, 0.7]$  such that  $\min_{j,k \in \{1, \dots, 10\}} \{|c_j - c_k|\} > 0.4$  and  $n$  radii  $R_j \in [0.1, 0.17]$ , and

changing each element of the matrix from 0 to 1 if and only if the distance  $c_j$  was less than  $R_j$  for some  $j$ . Out of 170 different images, 10 were included into the training set and the rest 160 into the test set. Augmented version of the training set with 40 images was then created by adding three versions of each image in the original training set by mapping them with the composed mapping  $f^{-1} \circ v \circ g \circ f$ , where  $f, g, v$  are as in (2.5)-(2.9) for  $\alpha = 0.1 + 0.1i$  and  $k = \pi/3$ ,  $\alpha = 0.1 + 0.3i$  and  $k = \pi$ , and  $\alpha = 0.3 + 0.3i$  and  $k = 3\pi/2$ , as shown in Figure 2. The final images were scaled to the size of  $128 \times 128$  pixels.

**4.2. Convolutional neural network.** The CNN used here is the same as in [9]. It uses U-Net architecture introduced in [14] and therefore contains first an expanding path and then a contracting path. The expanding path consist of four sequences, each of which contains two convolutions and one pooling operation, while the contracting path has four dense layers. The activation function of the last layer is a linear function and, for all the other layers, the ReLu function is used. The CNN was trained on 130 epochs for both augmented and non-augmented data by using Adam as the optimizer, the mean squared error (MSE) as the loss function with learning rate of 0.001, and validation split of 30%.

**4.3. Methods.** The CNN is first initialized, trained with the non-augmented data set, and used to predict the values of the test set. Then we compute the squared error between the predicted number of disks and the real number of disks for each image of the test set. After that, the CNN is re-initialized to its initial state and the experiment is re-run by using the augmented training data instead. The two methods are compared by computing the MSE as the mean value of the squared errors and, to see if the difference in these means is statistically significant or not, the Student's t-test is performed for the distributions of the squared errors.

**4.4. Results.** When the CNN was trained on non-augmented data, the MSE was 2.381 for the predictions of the test set. For the augmented data, the MSE was 1.742 in the test set. In other words, the MSE was 26.8% smaller for predictions obtained by using augmentation in the training. According the Student's t-test between the squared errors of the predictions from the non-augmented and the augmented model, the difference between the MSEs was statistically significant with a p-value 0.0360. Pearson's correlation coefficient between the predictions on the test set by the non-augmented CNN and the real numbers of disks is 0.884, while the corresponding correlation between the predictions from the augmented CNN and the real values is 0.924.

## 5. DISCUSSION

Firstly, it must be noted that the experiment above is very simplified example and better results could be obtained by building a suitable algorithm instead of using a CNN. However, there are numerous practical reasons why a CNN that recognizes certain unusual disk-shaped areas are useful. In fact, this experiment was inspired by training CNNs to detect tumors from tomography images of cancer patients.

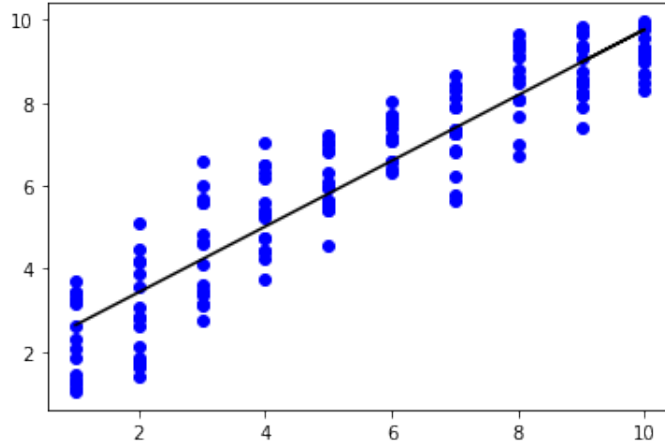


FIGURE 3. The predictions of the augmented CNN against the real values of the test set with the least squares regression line. The slope of the line is 0.793 and the intercept is 1.846. The correlation between the predictions and the real values is 0.924.

It also should be taken into account that this method is quite complicated and designed for situations where the typical transformations cannot be used. For instance, if some of the disks would be so close to edges of the images in our experiment that they would be cropped completely or partially out when the square-shaped images are directly rotated and re-calculating their number is not possible, using this new method rather than the usual rotation is justified. Given how commonly CNNs are used nowadays, there are likely many practical examples of cases where information could be lost if the typical rotation is used. Note that these mappings can be also extended to map any rectangle-shaped image into a disk or vice versa because the rectangle can be very easily stretched into a square.

Another reason for using this method is wanting to utilize the properties of the Möbius transformation in particular. Because of this mapping, the images change in more complicated ways under this augmentation method than they do in simple rotations. We can see that the right-most disk in Figure 2(D) is larger than any of the disks in the original image in Figure 2(A). By increasing the absolute value of the point  $\alpha$  used to define the Möbius transformation, the differences between the images before and after the composed mapping are also increased. Still, all these disks stay circular because Möbius transformations can only map circles into lines or circles and the disks stay inside the edges of the image.

One alternative method is using general adversarial network (GAN) augmentation first introduced in 2014 by Goodfellow et al. [8]. GANs are a class of neural networks that generate synthetic samples resembling the real images of the original data set. However, it might be difficult to predict what sort of augmented data GANs produce while the use of conformal mappings only distort the images. This means that the augmentation based on

the conformal mappings preserves the number of disks in the images of the data set used here, while GANs might change the number of disks. Furthermore, GANs also require some amount of data so that they can be trained for their work, while there amount of the data does not affect how the images change under the conformal mappings.

## 6. CONCLUSION

We used conformal mappings to create a new way to augment the image data of a CNN and, according to our result, this method both works and produces better predictions than a CNN trained with non-augmented data set.

## REFERENCES

1. M. Abramowitz and I.A. Stegun, *Handbook of mathematical functions*, 10th ed., Dover, New York, 1972.
2. M. Abadi, A. Agarwal, P. Barham, E. Brevdo, Z. Chen, C. Citro, G.S. Corrado, ..., X. Zheng. (2015). TensorFlow: Large-scale machine learning on heterogeneous systems.
3. G. D. Anderson, M. K. Vamanamurthy, M. Vuorinen, *Conformal invariants, inequalities and quasiconformal maps*. Canadian Mathematical Society Series of Monographs and Advanced Texts. A Wiley-Interscience Publication. J. Wiley, 1997.
4. H. Bateman, A. Erdelyi, *Higher transcendental functions*. Vol. 1, 1953.
5. F. Chollet et al. (2015). Keras. GitHub.
6. H. Dalichau, *Conformal Mapping and Elliptic Functions*. München, <http://dateiena.harald-dalichau.de/spcm/pref11.pdf> (2006).
7. T.A. Driscoll, L.N. Trefethen, *Schwarz-Christoffel Mapping*. Cambridge Monographs on Applied and Computational Mathematics. Cambridge University Press, 2002.
8. I. Goodfellow, J. Pouget-Abadie, M. Mirza, B. Xu, D. Warde-Farley, S. Ozair, A. Courville, Y. Bengio. (2014). Generative adversarial nets. In: *Advances in neural information processing systems*. pp. 2672–80
9. H. Hellström, J. Lienes, O. Rainio, S. Malaspina, J. Kemppainen, R. Klén. (2022). Classification of head and neck cancer from PET images using convolutional neural networks. [Manuscript].
10. H. Kober, *Dictionary of conformal representations*. Vol. 2. Dover, New York, (1957).
11. P.K. Kythe, *Handbook of conformal mappings and applications*, CRC Press, 2019.
12. I. Moiseev, Elliptic functions for Matlab and Octave, GitHub repository, doi: <http://dx.doi.org/10.5281/zenodo.48264>, 2008.
13. F.W.J. Olver, D.W. Lozier, R.F. Boisvert, and C.W. Clark, *NIST handbook of mathematical functions*, Cambridge university press, Cambridge, 2010.
14. O. Ronneberger, P. Fischer, T. Brox. (2015). U-Net: Convolutional Networks for Biomedical Image Segmentation (pp. 234–241). In: Navab N., Hornegger J., Wells W., Frangi A. (eds) Medical Image Computing and Computer-Assisted Intervention – MICCAI 2015. MICCAI 2015. Lecture Notes in Computer Science, vol 9351. Springer, Cham.
15. G. van Rossum, F.L. Drake (2009). Python 3 Reference Manual. CreateSpace.
16. P. Virtanen, R. Gommers, T.E. Oliphant, M. Haberland, T. Reddy, D. Cournapeau, E. Burovski, P. Peterson, W. Weckesser, J. Bright, S.J. van der Walt, M. Brett, J. Wilson, K. Jarrod Millman, N. Mayorov, A.R.J. Nelson, E. Jones, R. Kern, E. Larson, C.J. Carey, Í. Polat, Y. Feng, E.W. Moore, J. VanderPlas, D. Laxalde, J. Perktold, R. Cimrman, I. Henriksen, E.A. Quintero, C.R. Harris, A.M. Archibald, A.H. Ribeiro, F. Pedregosa, P. van Mulbregt, and SciPy 1.0 Contributors. (2020) SciPy 1.0: Fundamental Algorithms for Scientific Computing in Python. *Nature Methods*, 17(3), 261–272.